Flow and transport modeling of a tracer isotope experiment at B2 LEO using integrated and distributed multisensor observation data

POSTER H13E-1165

Carlotta Scudeler[1,2], Luke Pangle[3,4], Damiano Pasetto[2], Guo-Yue Niu[3,4], Claudio Paniconi[1], Mario Putti[2], Peter A. Troch[3,4]

1 Institut National de la Recherche Scientifique, Centre Eau Terre Environnement (INRS-ETE), Quebec City, Canada
2 Department of Mathematics, Università di Padova, Padua, Italy
3 Biosphere 2 – Earth Science, University of Arizona, Tucson, USA
4 Department of Hydrology and Water Resources, University of Arizona, Tucson, USA

carlotta.scudeler@gmail.com

Abstract: An emerging challenge in hydrological modeling is that of simulating multiple responses, both integrated and distributed, based on multivariate observations. In this work we analyze the tracer experiment conducted at the Landscape Evolution Observatory (LEO) at the Biosphere 2 (B2) [1] by way of flow and transport numerical simulations. Deuterium (^2H) was introduced into the system via the rainfall simulator at a known rate and concentration. The collected data consist of spatially integrated and point-scale responses for both flow and transport, measured at fine temporal resolution. Modeling is used to interpret the observation data and to study the water and solute dynamics over the hillslope. It is also used to examine some numerical issues connected to mass conservation and solute exchange across the soil/atmosphere boundary.

1) Description of the tracer experiment

From April 13 to 30, 2013 a flow and tracer experiment was carried out on the east hillslope of B2 (Fig.1):

- 3 pulses of rain for a total of about 16 hours at a constant rate of 12 mm/h (Fig. 2). The water of the second pulse has no ^2H deficit, while for the first and third ones, as for the water initially in the system, the deficit is -60 ‰.
- The concentration (c) plotted in Fig. 2 is relative to the maximum deficit -60 ‰: c=0 ➔ deficit of ^2H in water is maximal; c=1 ➔ no ^2H deficit in water.
- Estimated initial condition (IC): 26 m^3 total storage, unsaturated conditions.

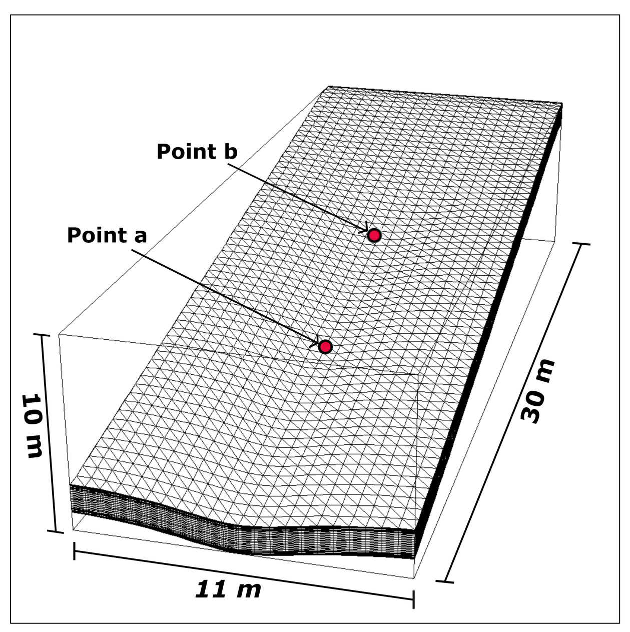

Fig. 1. 3D numerical grid for the LEO hillslope.

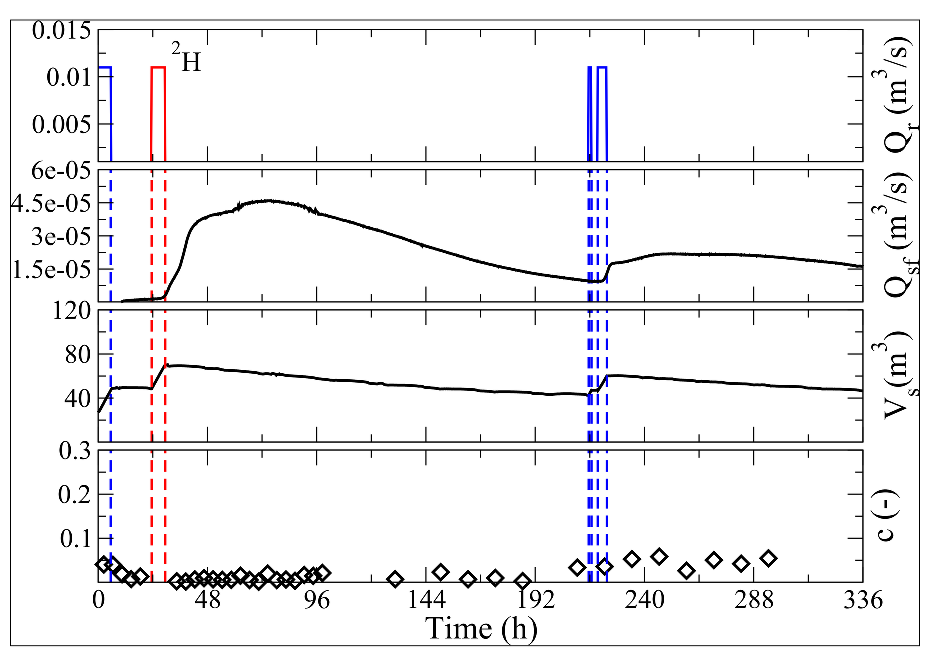

Fig. 2. Measured rain input (Q_r), seepage outflow (Q_{sf}), total internal storage (V_s), and average concentration (c) at the seepage face (SF).

Observations (Fig. 2): the water table is low. Low Q_{sf}. No surface runoff. Very low average c at SF. Estimate of evaporation rate (high) is obtained from mass balance calculations.
Data we look at: Integrated responses for flow (Q_{sf}, V_s) and for transport (average c at SF); point-scale for flow (volumetric water content θ profiles) and for transport (breakthrough curves) relative to point a and point b (Fig.1) at 5, 20, 50, and 85 cm depth from surface.

2) Hydrological model

- CATchment HYdrology model (CATHY) [2,3] for Richards equation (eq. 1) and for the solution of the advective-dispersive equation for solute transport in partially saturated porous media (eq. 3). Both flow and transport router are finite-element based

Flow equation (eq. 1) and corresponding boundary conditions (BC) (eq. 2)

$$S_w S_s \frac{\partial \psi}{\partial t} + \phi \frac{\partial S_w}{\partial t} = -\nabla v + q \qquad (1)$$

$$\psi = \psi_D \quad on \quad \Gamma_D^f \qquad q_n^f = v \cdot n \quad on \quad \Gamma_n^f \qquad (2)$$

where Sw = water saturation, S_s = elastic storage coefficient, ψ = pressure head, t = time, φ =porosity, v = Darcy flux, q = sink/source term, q^f_n = Neumann flux for flow, n = outward normal vector, Γ^f_D and Γ^f_n = Dirichlet and Neumann boundaries, respectively, for flow.

Transport equation (eq. 3) and corresponding BC (eq. 4)

$$\frac{\partial(\phi S_w c)}{\partial t} = \nabla \cdot [-vc + D\nabla c] \qquad (3)$$

$$c = c_D \quad on \quad \Gamma_D^t \qquad q_n^t = -D\nabla c \cdot n \quad on \quad \Gamma_n^t$$

$$q_c^t = (vc - D\nabla c) \cdot n \quad on \quad \Gamma_c^t \qquad (4)$$

where D = dispersion tensor, q^t_n and q^t_c = Neumann and Cauchy fluxes, Γ^t_D, Γ^t_n and Γ^t_c = Dirichlet, Neumann, and Cauchy boundaries for transport.

Treatment of atmospheric boundary conditions

	1st and 3rd pulses	2nd pulse	evaporation
FLOW	prescribed q^f_n	prescribed q^f_n	prescribed q^f_n
TRANSPORT	q^t_c=0	*prescribed* q^t_c with c=1	- q^t_n=0 ➔ ^2H in solution evaporates with water - sink term for evaporation + ^2H injection with correction term added in eq. 3 ➔ ^2H does not evaporate - if ^2H partial injection ➔ just a part of ^2H evaporates

Tab. 1. Atmospheric boundary conditions for flow and transport implemented to model the experiment.

3) Integrated flow response

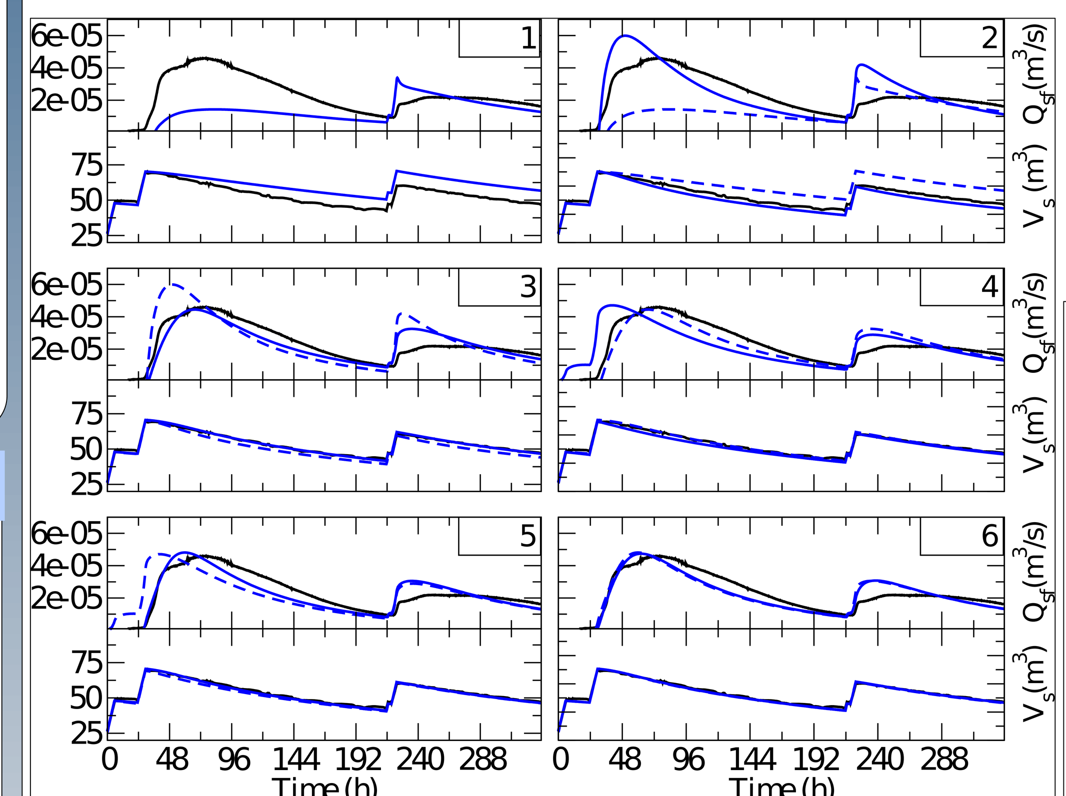

Fig. 3. On each graph: measured (black line) and modeled (blue line) for Q_{sf}, (top) and V_s (bottom). The results are plotted as a progression from graph 1 to graph 6. The blue dashed lines represent the previous calculated responses (e.g., for graph 2 it is the one of graph 1).

1 Homogeneity
1➔2 Add anisotropy
2➔3 Add heterogeneity at SF [3]
3➔4 Uniform IC ➔IC from steady state (SS) simulation
4➔5 IC from SS simulation ➔IC with match of measurements
5➔6 Uniform ➔spatially distributed rainfall

Results Fig. 3: water balance partitioning between Q_{sf} and V_s affected by anisotropy, by heterogeneity, and by the distribution of IC. Graph 6 in Fig. 3 shows the model results that best capture the measured system response. These results take into account the same soil parameters estimated in [4], with the addition of anisotropy, and are used as input for the transport model.

4) Integrated transport response

Different values of longitudinal dispersivity (α_l) are tested (the transverse dipsersivity, α_t, is maintained one order of magnitude smaller for all cases).

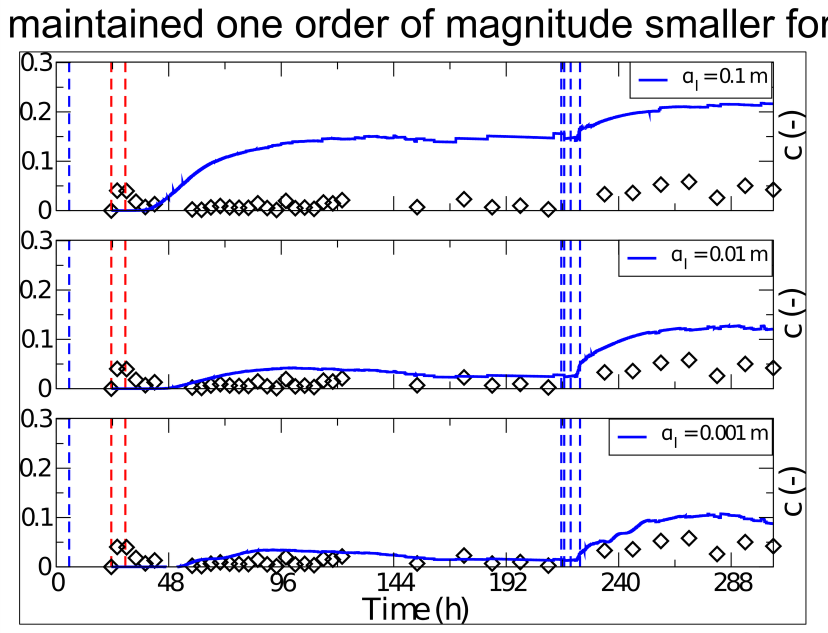

Fig. 4. Measured (black diamonds) and modeled (blue lines) average c at SF for different α.

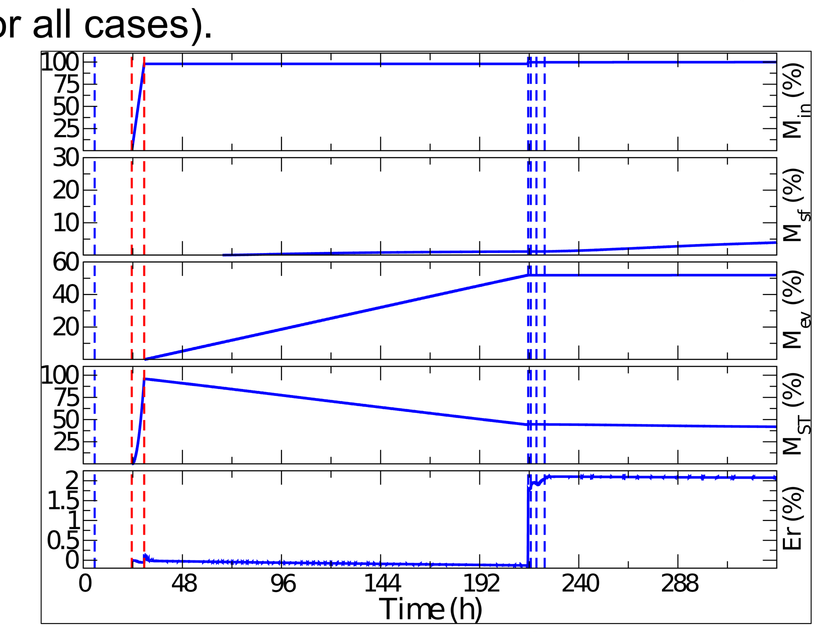

Fig. 5. Model mass balance results for α_l=0.001 m. From top: cumulative mass injected (M_{in}), mass outflow from SF (M_{sf}), mass evaporated (M_{ev}), and mass stored (M_{ST}), all expressed as a % of M_{in}. Bottom graph: $Er=(M_{in}-M_{sf}-M_{ev}-M_{ST})$.

Results Figs. 4 and 5: for the smallest α_l used, the model response is very close to the observations (bottom graph of Fig. 4). But looking at Fig. 5, M_{ev} is more than half of the total mass injected. To address this problem, we perform two additional simulations:
1) evaporation of water alone (all the solute stays in the system)
2) evaporation with fractionation [5] (some solute stays in the system)

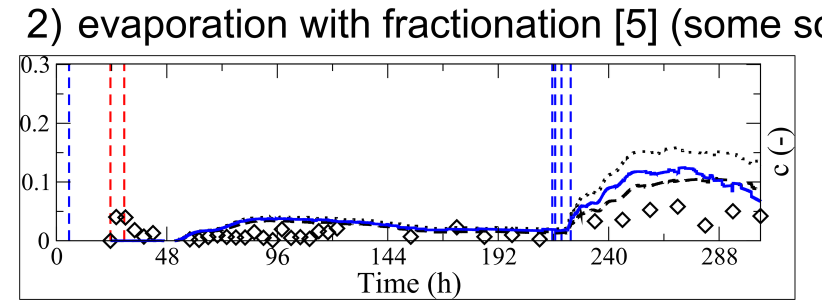

Fig. 6. Measured (black diamonds) and modeled c at SF for the case in which all (black dashed line), a portion (solid blue line), or no (black points) ^2H mass evaporates with water.

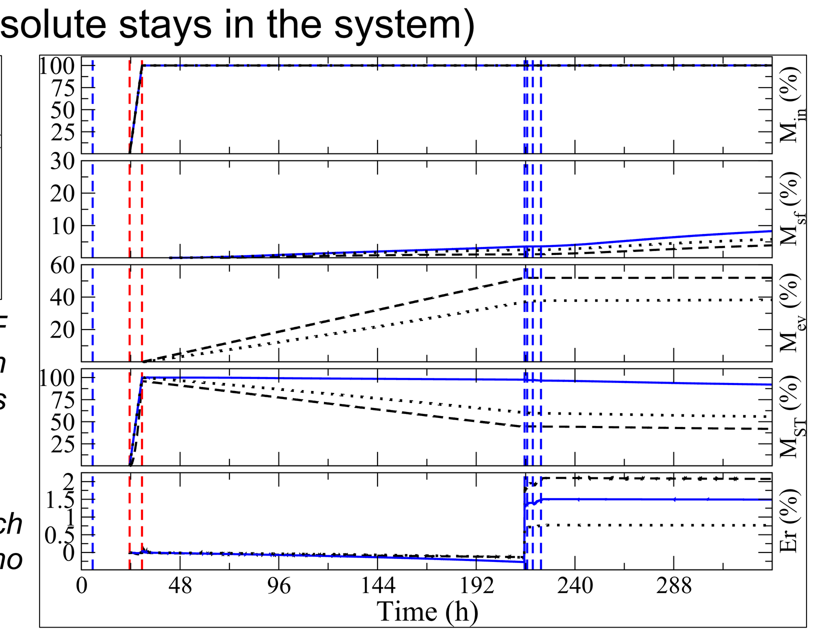

Fig. 7. Model mass balance results for the case in which all (black dashed line), a portion (solid blue line), or no (black points) ^2H mass evaporates with water.

Results Figs. 6 and 7: very different M_{ev} and M_{ST} (Fig. 7) for the three simulations; differences not so evident for M_{sf} and c at SF (Fig. 6), implying that the isotope does not percolate very far (deep) into the hillslope. We cannot know what happens in reality since the soil evaporation isotopic composition has not been measured.

5) Point-scale flow response

For the simulation that best retrieves the integrated flow response (graph 6 of Fig. 3 in section 3) in Fig. 8 we look at the θ profiles obtained by averaging the observations/model results at the sensor locations found at a specific depth from surface.

Fig. 8. Measured (solid black lines) and modeled solid (blue lines) average θ profiles at 5, 20, 50, and 85 cm depth (from top to bottom). In each graph the deviation from the mean is reported as a double dashed line (blue for the model and black for the measurements).

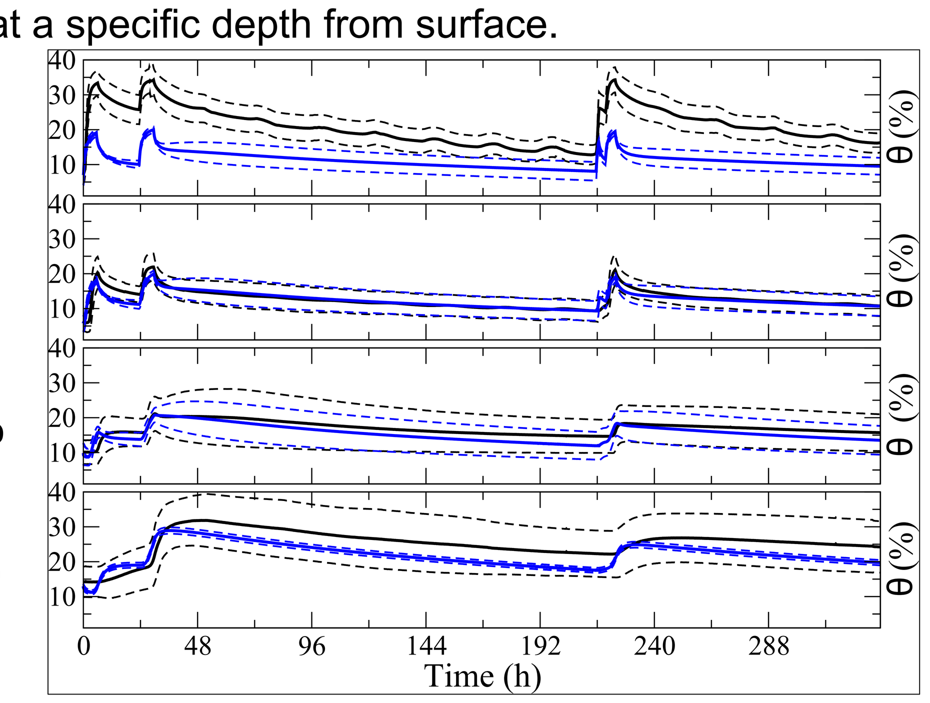

Results of Fig. 8: the model at 5 and 85 cm underestimates on average the observed response. To address this problem we increase the retention capacity (by decreasing the value of *VGN*, the n parameter of the van Genuchten curves) from the setting *VGN* = 2.26 used here.

	Layer 1	Layer 2	Layer 3	Layer 4
Depth	0-10 cm	10-32 cm	32-68 cm	68-100 cm
VGN	1.8	2.26	2	1.9

Tab. 2. Soil parameterization for VGN used to obtain the results reported in Fig. 9.

Results of Fig. 9: model results for the average θ profiles obtained by varying *VGN* improve significantly at 5, 50, and 85 cm depth (at 20 cm *VGN* was unchanged with respect to Fig. 8).

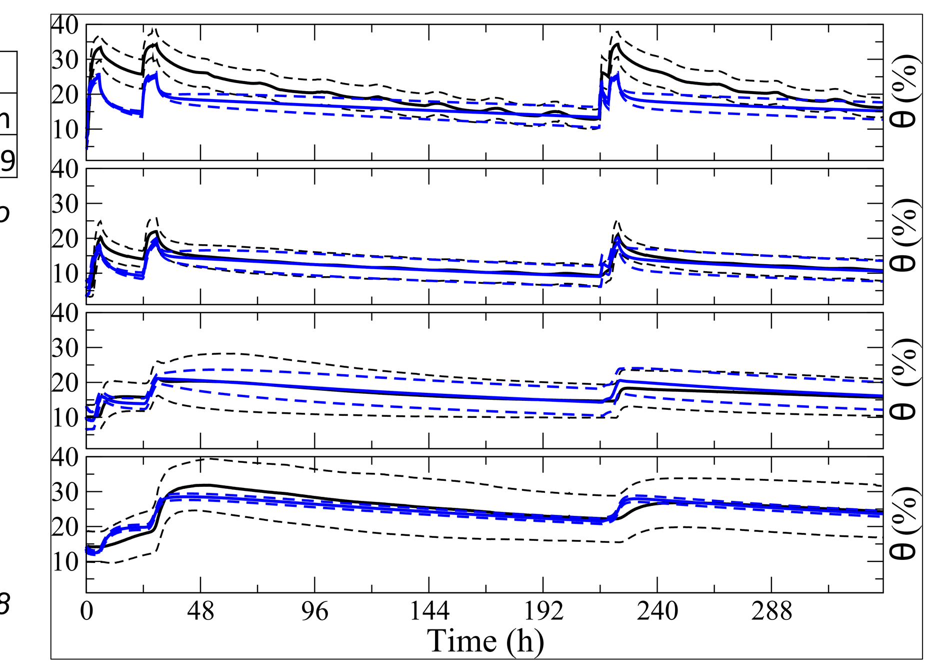

Fig. 9. Average θ profiles as reported in Fig. 8 for the case of varying VGN.

6) Point-scale transport response

With the flow results reported in graph 6 of Fig. 3 and in Fig. 8 (for *VGN* = 2.26 everywhere) and for the flow results shown in Fig. 9 (obtained by varying *VGN*) we run the transport model (configuration of Fig. 4 with α_l =0.001).

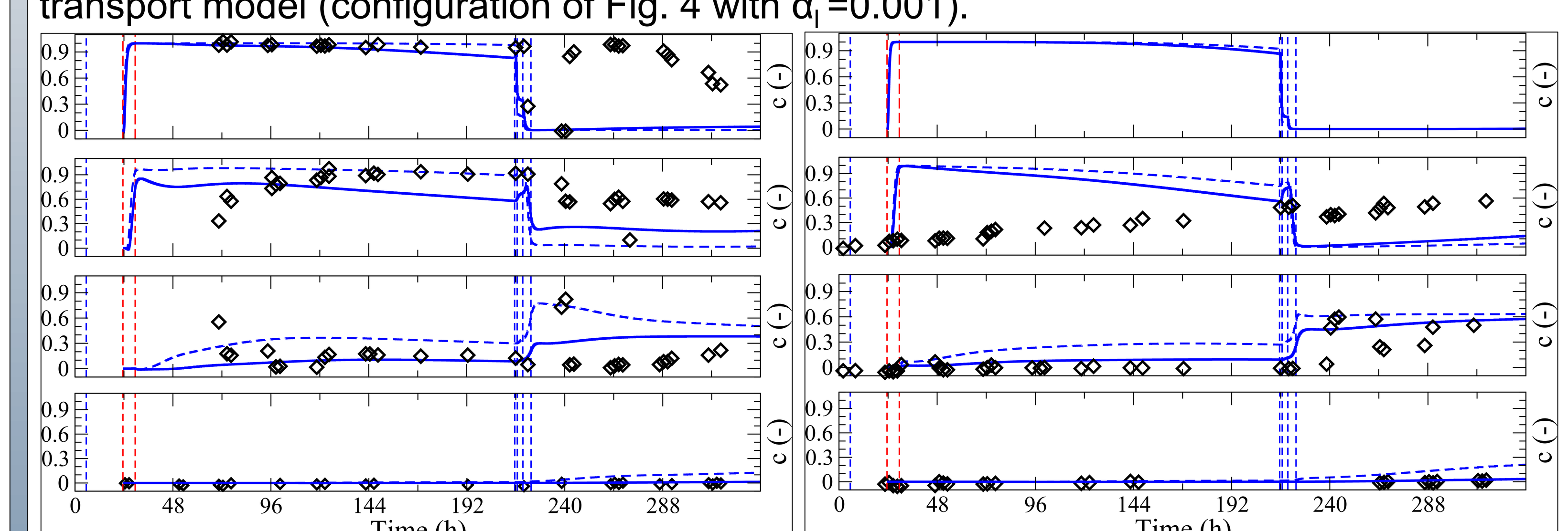

Fig. 10 Measured (black diamonds) and modeled c for varying VGN (solid blue lines) and for VGN = 2.26 (dashed blue lines) at 5, 20, 50, and 85 cm depth from surface (top to bottom graphs) for point a (left) and point b (right). The location of points a and b is shown in Fig. 1.

Results of Fig. 10: the results for the varying *VGN* case seem slightly better than the constant *VGN* simulation. Overall however neither case adequately captures the point-scale transport response, especially for the layers closer to the surface. A parameterization refinement appears necessary here just as was the case in passing from the integrated to the point-scale flow analyses.

Conclusions: The first tracer experiment performed at LEO presents many opportunities to advance and test our ability to model complex processes (coupled flow and transport, advection vs dispersion, water and solute exchanges between soil and atmosphere, etc). In this study we demonstrate how complex the problem of model parameterization is when dealing with multiple processes (flow, transport, surface, subsurface, etc) and multivariate observations (soil moisture, outflow, solute concentration, mass storage, etc) of both integrated and distributed nature.

References

[1] T. Huxman, P. Troch, J. Chorover, D. Breshears, S. Saleska, J. Pelletier, X. Zeng, and J. Espeleta. The hills are alive: interdisciplinary earth science at biosphere 2. *EOS*, 90:120, 2009.
[2] M. Camporese, C. Paniconi, M. Putti, and S. Orlandini. Surface-subsurface flow modeling with path-based runoff routing, boundary condition-based coupling, and assimilation of multisource observation data. *Water Resources Research,* 46:W02512, 2010.
[3] S. Weill, A. Mazzia, M. Putti, and C. Paniconi. Coupling water flow and solute transport into a physically-based surface-subsurface hydrological model. *Advances in Water Resources,* 34:128–136, 2011.
[4] G.-Y. Niu, D. Pasetto, C. Scudeler, C. Paniconi, M. Putti, P. Troch, S. B. DeLong, K. Dontsova, L. Pangle, D. D. Breshears, J. Chorover, T. E. Huxman, J. Pelletier, S. R. Saleska, and X. Zeng. Incipient subsurface heterogeneity and its effect on overland flow generation–Insight from a modeling study of the first experiment at the Biosphere 2 Landscape Evolution Observatory. *Hydrology and Earth System Sciences,* 10:12615–12641, 2014.
[5] C. Barnes and G. Allison. Tracing of water movement in the unsaturated zone using stable isotopes of hydrogen and oxygen. *Journal of Hydrology,* 100:143–176, 1988.